Numer. Math. Theor. Meth. Appl.
doi: 10.4208/nmtma.OA-2025-0101

Vol. **19**, No. 1, pp. 219-239
February 2026

The Method of Fundamental Solutions for Optical Fluorescence Tomography

Andreas Karageorghis[1,*] and Daniel Lesnic[2]

[1] *Department of Mathematics and Statistics, University of Cyprus, Nicosia 1678, Cyprus*
[2] *Department of Applied Mathematics, University of Leeds, Leeds LS2 9JT, UK*

Received 10 September 2025; Accepted (in revised version) 2 December 2025

Abstract. In this paper, the method of fundamental solutions (MFS) is first developed for solving direct problems in bi-layer materials in the biomedical field of optical fluorescence. The governing system of second-order linear partial differential equations (PDEs) for the emission and excitation fluences is transformed into a single fourth-order PDE with appropriate boundary and interface matching conditions. The MFS is subsequently further developed, in conjunction with a constrained minimization regularization procedure, to solve nonlinear inverse optical fluorescence tomography problems. Numerical results confirm the accuracy, stability and versatility of the proposed meshless technique.

AMS subject classifications: Primary 65N35; Secondary 65N21, 65N38

Key words: Optical fluorescence, method of fundamental solutions, bi-layer materials, elliptic equations.

1. Introduction

Optical fluorescence tomography (OFT) has emerged as an exciting molecular imaging lymph node or cancer detection technique. Through the injection of a fluorescent dye that directly targets specific tissues, OFT increases the signal-to-noise ratio detection when compared to the more well-known diffusive optical tomography (DOT) [2]. In several papers [2,14–17], Joshi and his co-workers developed a mathematical model for OFT governing the excitation light and the subsequent propagation of fluorescence light through a tissue medium [10].

In an earlier study [20], we proposed the method of fundamental solutions, as a suitable meshless method for solving the direct linear optical fluorescence boundary value problem (BVP). In the current paper, we advance the MFS to solving this BVP in

*Corresponding author. *Email addresses:* andreask@ucy.ac.cy (A. Karageorghis), D.Lesnic@leeds.ac.uk (D. Lesnic)

a bi-layer material and the associated inverse nonlinear geometric problem. The latter requires the reconstruction of an unknown inclusion modelling an anomaly/defect that may be present within a biological tissue.

The plan of the paper is as follows. In Section 2, we introduce the governing optical fluorescence mathematical model based on a coupled system of two elliptic partial differential equations subjected to Robin third-kind convective boundary conditions (BCs) in a bi-layer material consisting of an anomaly surrounded by a healthy tissue. In Section 3, we introduce the MFS for a bi-material by extending our previous work [20] concerned with single-layer materials. Numerical experiments for the direct BVP of optical fluorescence in a bi-layer material are conducted in Section 4. In Section 5, the inverse geometric nonlinear OFT problem is formulated and solved numerically using the MFS combined with a constrained minimization technique whose objective function needs to be further regularized in order to achieve stability of the anomaly reconstruction. Finally, in Section 6 we highlight the conclusions of the paper.

2. Mathematical model

In non-dimensional form, the photon propagation in a bounded tissue Ω, in the frequency domain, is governed by the following system of PDEs [2, 16, 20]:

$$\Delta u - \alpha_{\rm x} u = 0 \qquad \text{in } \Omega, \tag{2.1a}$$

$$\Delta v - \alpha_{\rm m} v = -B_{\rm x} u \quad \text{in } \Omega, \tag{2.1b}$$

where u and v are the excitation and emission light fluence, respectively,

$$\begin{aligned}
\alpha_{\rm x} &= 3L^2(\mu_{\rm axi} + \mu_{\rm axf} + {\rm i}\omega/c)(\mu_{\rm axi} + \mu_{\rm axf} + \mu'_{\rm sx}),\\
\alpha_{\rm m} &= 3L^2(\mu_{\rm ami} + \mu_{\rm amf} + {\rm i}\omega/c)(\mu_{\rm ami} + \mu_{\rm amf} + \mu'_{\rm sm}),\\
B_{\rm x} &= \frac{3L^2\varphi\mu_{\rm axf}(\mu_{\rm ami} + \mu_{\rm amf} + \mu'_{\rm sm})}{1 - {\rm i}\omega\tau},
\end{aligned} \tag{2.2}$$

τ is the life time of the fluorosphore, φ is the probability of the re-emitted excitation fluence after dye absorption, L is a characteristic dimension of the spatial tissue domain, ω is the modulation frequency, ${\rm i} = \sqrt{-1}$, c is the speed of light, $\mu'_{\rm sx}, \mu'_{\rm sm}, \mu_{\rm axi}, \mu_{\rm ami}$ and $\mu_{\rm axf}, \mu_{\rm amf}$ are coefficients characterizing reduced scattering, absorption due to endogenous chromophores and absorption due to exogenous fluorosphore at the excitation and emission wavelengths, respectively.

The BCs associated to (2.1a) and (2.1b) are of Robin type and given by [2, 16, 20]

$$2\mathcal{D}_{\rm x}\frac{\partial u}{\partial n} + \gamma u + S = 0 \quad \text{on } \partial\Omega, \tag{2.3a}$$

$$2\mathcal{D}_{\rm m}\frac{\partial v}{\partial n} + \gamma v = 0 \qquad \text{on } \partial\Omega, \tag{2.3b}$$

where $\boldsymbol{n}$ is the outward unit normal vector to $\partial\Omega$, S is an excitation source, γ is a constant depending on the optical refractive index mismatch at the boundary $\partial\Omega$, [10], and

$$\mathcal{D}_{\rm x} = \frac{1}{3L\left(\mu_{\rm axi} + \mu_{\rm axf} + \mu'_{\rm sx}\right)}, \quad \mathcal{D}_{\rm m} = \frac{1}{3L\left(\mu_{\rm ami} + \mu_{\rm amf} + \mu'_{\rm sm}\right)}. \tag{2.4}$$

We assume that the absorption coefficients $\mu_{\rm axf}$ and $\mu_{\rm amf}$ due to exogenous fluorosphore at the excitation and emission wavelengths, respectively, are piecewise constant given by

$$\begin{aligned} \mu_{\rm axf}(\boldsymbol{x}) &= \mu^{(2)}_{\rm axf} + \left(\mu^{(1)}_{\rm axf} - \mu^{(2)}_{\rm axf}\right)\chi_{\rm D}(\boldsymbol{x}), \qquad \boldsymbol{x} \in \Omega, \\ \mu_{\rm amf}(\boldsymbol{x}) &= \mu^{(2)}_{\rm amf} + \left(\mu^{(1)}_{\rm amf} - \mu^{(2)}_{\rm amf}\right)\chi_{\rm D}(\boldsymbol{x}), \quad \boldsymbol{x} \in \Omega, \end{aligned} \tag{2.5}$$

where $\chi_{\rm D}$ is the characteristic function of an inclusion D compactly contained in the host medium Ω such that $\Omega\backslash$D is connected. The expressions in (2.5) can be rewritten as

$$\mu_{\rm axf}(\boldsymbol{x}) = \begin{cases} \mu^{(1)}_{\rm axf}, & \text{if} \quad \boldsymbol{x} \in {\rm D}, \\ \mu^{(2)}_{\rm axf}, & \text{if} \quad \boldsymbol{x} \in \Omega\backslash{\rm D}, \end{cases} \quad \mu_{\rm amf}(\boldsymbol{x}) = \begin{cases} \mu^{(1)}_{\rm amf}, & \text{if} \quad \boldsymbol{x} \in {\rm D}, \\ \mu^{(2)}_{\rm amf}, & \text{if} \quad \boldsymbol{x} \in \Omega\backslash{\rm D}. \end{cases} \tag{2.6}$$

These expressions yield the corresponding piecewise constant functions $\alpha^{(\ell)}_{\rm x}, \alpha^{(\ell)}_{\rm m}$ and $B^{(\ell)}_{\rm x}$ for $\ell = 1, 2$, defined from Eqs. (2.2). They also yield the bi-domain formulations of Eqs. (2.1a) and (2.1b) for the functions $u^{(1)}, v^{(1)}$ in D and $u^{(2)}, v^{(2)}$ in $\Omega\backslash$D satisfying

$$\Delta u^{(1)} - \alpha^{(1)}_{\rm x} u^{(1)} = 0 \qquad \text{in D}, \tag{2.7a}$$

$$\Delta v^{(1)} - \alpha^{(1)}_{\rm m} v^{(1)} = -B^{(1)}_{\rm x} u^{(1)} \quad \text{in D}, \tag{2.7b}$$

$$\Delta u^{(2)} - \alpha^{(2)}_{\rm x} u^{(2)} = 0 \qquad \text{in } \Omega\backslash\overline{\rm D}, \tag{2.7c}$$

$$\Delta v^{(2)} - \alpha^{(2)}_{\rm m} v^{(2)} = -B^{(2)}_{\rm x} u^{(2)} \quad \text{in } \Omega\backslash\overline{\rm D}, \tag{2.7d}$$

linked through the interface conditions (ICs) on ∂D given by

$$u^{(1)} = u^{(2)} \qquad \text{on } \partial{\rm D}, \tag{2.8a}$$

$$v^{(1)} = v^{(2)} \qquad \text{on } \partial{\rm D}, \tag{2.8b}$$

$$\frac{\partial u^{(1)}}{\partial {\rm n}} = \frac{\partial u^{(2)}}{\partial {\rm n}} \quad \text{on } \partial{\rm D}, \tag{2.8c}$$

$$\frac{\partial v^{(1)}}{\partial {\rm n}} = \frac{\partial v^{(2)}}{\partial {\rm n}} \quad \text{on } \partial{\rm D}, \tag{2.8d}$$

where $\mathbf{n}$ is the inward unit normal vector to ∂D, see also the geometry of the problem depicted in Fig. 1. Finally, BCs (2.3a)-(2.3b) on $\partial\Omega$ recast as

$$2\mathcal{D}_{\rm x}\frac{\partial u^{(2)}}{\partial n} + \gamma u^{(2)} + S = 0 \quad \text{on } \partial\Omega, \tag{2.9a}$$

$$2\mathcal{D}_{\rm m}\frac{\partial v^{(2)}}{\partial n} + \gamma v^{(2)} = 0 \qquad \text{on } \partial\Omega. \tag{2.9b}$$

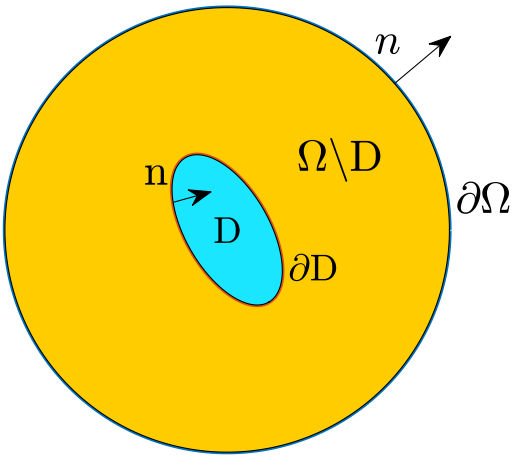

Figure 1: Geometry of problem.

In the past, the MFS was applied to bi-layered homogeneous materials undergoing excitations in electrostatics governed by Laplace's equation, in steady-state bioheat transfer governed by the modified Helmholtz equation and in unsteady heat conduction governed by the transient heat equation in [4, 5, 13], respectively. Here, we develop the MFS for bi-layered piecewise constant materials undergoing optical fluorescence excitations for both direct problem simulations and inverse tomographic inspection.

3. The MFS for bimaterial in optical fluorescence

3.1. The MFS for the excitation fluence

We consider the solution of the BVP consisting of PDEs (2.7a) and (2.7c), the ICs (2.8a) and (2.8c), and the BC (2.9a). We first describe the MFS for a function satisfying Eq. (2.7a), as a linear combination of fundamental solutions of the complex Helmholtz equation

$$\Delta\Phi - \alpha\Phi = 0 \quad \text{with} \quad \alpha \in \mathbb{C}, \tag{3.1}$$

which in two dimensions is given by [11]

$$\Phi(\boldsymbol{x};\boldsymbol{\xi}) = -\frac{1}{2\pi} K_0\left(\sqrt{\alpha}|\boldsymbol{x}-\boldsymbol{\xi}|\right), \tag{3.2}$$

where K_0 is the modified Bessel function of the second kind of order zero, namely,

$$u^{(1)}(\boldsymbol{x}) \approx \tilde{u}^{(1)}(\boldsymbol{x}) = -\frac{1}{2\pi}\sum_{j=1}^{N} c_j^{(1)} K_0\left(\sqrt{\alpha_{\mathrm{x}}^{(1)}}|\boldsymbol{x}-\boldsymbol{\xi}_j^{(1)}|\right), \quad \boldsymbol{x} \in \overline{\mathrm{D}}, \tag{3.3}$$

where $(\boldsymbol{\xi}_j^{(1)})_{j=\overline{1,N}}$ are sources placed outside $\overline{\mathrm{D}}$ (such that $u_N^{(1)}$ satisfies Eq. (2.7a) in D). Similarly, we approximate a function satisfying (2.7c) by

$$u^{(2)}(\boldsymbol{x}) \approx \tilde{u}^{(2)}(\boldsymbol{x}) = -\frac{1}{2\pi}\sum_{j=1}^{M} c_j^{(2)} K_0\left(\sqrt{\alpha_{\mathrm{x}}^{(2)}}\big|\boldsymbol{x}-\boldsymbol{\xi}_j^{(2)}\big|\right), \quad \boldsymbol{x}\in\overline{\Omega}\backslash\mathrm{D}, \tag{3.4}$$

where $(\boldsymbol{\xi}_j^{(2)})_{j=\overline{1,M}}$ are sources placed outside $\overline{\Omega}\backslash\mathrm{D}$, i.e. inside D and outside $\overline{\Omega}$.

In the MFS expansions (3.3) and (3.4), $(c_j^{(1)})_{j=\overline{1,N}}$ and $(c_j^{(2)})_{j=\overline{1,M}}$ are unknown complex coefficients that are determined by imposing the BC (2.3a) and the ICs (2.8a) and (2.8c) at the boundary points $(\boldsymbol{x}_k)_{k=\overline{1,N_1}} \in \partial\mathrm{D}$ and $(\boldsymbol{x}_k)_{k=\overline{N_1+1,N_1+N_2}} \in \partial\Omega$. This collocation process yields the following system of $2N_1+N_2$ complex equations in $N+M$ unknown complex coefficients:

$$\sum_{j=1}^{N} c_j^{(1)} K_0\Big(\sqrt{\alpha_{\mathrm{x}}^{(1)}}\big|\boldsymbol{x}_k-\boldsymbol{\xi}_j^{(1)}\big|\Big) = \sum_{j=1}^{M} c_j^{(2)} K_0\Big(\sqrt{\alpha_{\mathrm{x}}^{(2)}}\big|\boldsymbol{x}_k-\boldsymbol{\xi}_2^{(1)}\big|\Big), \quad k=\overline{1,N_1}, \tag{3.5a}$$

$$\begin{aligned}&\sqrt{\alpha_{\mathrm{x}}^{(1)}}\sum_{j=1}^{N} c_j^{(1)} K_1\left(\sqrt{\alpha_{\mathrm{x}}^{(1)}}\big|\boldsymbol{x}_k-\boldsymbol{\xi}_j^{(1)}\big|\right)\frac{(\boldsymbol{x}_k-\boldsymbol{\xi}_j^{(1)})\cdot\mathbf{n}(\boldsymbol{x}_k)}{|\boldsymbol{x}_k-\boldsymbol{\xi}_j^{(1)}|}\\ &= \sqrt{\alpha_{\mathrm{x}}^{(2)}}\sum_{j=1}^{M} c_j^{(2)} K_1\left(\sqrt{\alpha_{\mathrm{x}}^{(2)}}\big|\boldsymbol{x}_k-\boldsymbol{\xi}_j^{(2)}\big|\right)\frac{(\boldsymbol{x}_k-\boldsymbol{\xi}_j^{(2)})\cdot\mathbf{n}(\boldsymbol{x}_k)}{|\boldsymbol{x}_k-\boldsymbol{\xi}_j^{(2)}|}, \qquad k=\overline{1,N_1},\end{aligned} \tag{3.5b}$$

$$\begin{aligned}&\frac{\mathcal{D}_{\mathrm{x}}\sqrt{\alpha_{\mathrm{x}}^{(2)}}}{\pi}\sum_{j=1}^{M} c_j^{(2)} K_1\left(\sqrt{\alpha_{\mathrm{x}}^{(2)}}\big|\boldsymbol{x}_k-\boldsymbol{\xi}_j^{(2)}\big|\right)\frac{(\boldsymbol{x}_k-\boldsymbol{\xi}_j^{(2)})\cdot\boldsymbol{n}(\boldsymbol{x}_k)}{|\boldsymbol{x}_k-\boldsymbol{\xi}_j^{(2)}|}\\ &\quad+\frac{\gamma}{2\pi}\sum_{j=1}^{M} c_j^{(2)} K_0\left(\sqrt{\alpha_{\mathrm{x}}^{(2)}}\big|\boldsymbol{x}_k-\boldsymbol{\xi}_j^{(2)}\big|\right)+S(\boldsymbol{x}_k)=0, \quad k=\overline{N_1+1,N_1+N_2}.\end{aligned} \tag{3.5c}$$

This system may be written in compact form as

$$A\boldsymbol{c}=\boldsymbol{b}, \quad \text{where} \quad \boldsymbol{c}=\left(\left(c_j^{(1)}\right)_{j=\overline{1,N}},\left(c_j^{(2)}\right)_{j=\overline{1,M}}\right)^{\mathrm{T}}, \tag{3.6}$$

$$b_k=\begin{cases}0, & k=\overline{1,2N_1},\\ S(\boldsymbol{x}_{k-N_1}), & k=\overline{2N_1+1,2N_1+N_2},\end{cases} \tag{3.7}$$

$$A_{kj}=\begin{cases}K_0\left(\sqrt{\alpha_{\mathrm{x}}^{(1)}}\big|\boldsymbol{x}_k-\boldsymbol{\xi}_j^{(1)}\big|\right), & j=\overline{1,N},\\ -K_0\left(\sqrt{\alpha_{\mathrm{x}}^{(2)}}\big|\boldsymbol{x}_k-\boldsymbol{\xi}_{j-N}^{(2)}\big|\right), & j=\overline{N+1,N+M},\end{cases} \qquad k=\overline{1,N_1}, \tag{3.8a}$$

$$A_{kj}=\begin{cases}\sqrt{\alpha_{\rm x}^{(1)}}K_1\left(\sqrt{\alpha_{\rm x}^{(1)}}\left|\boldsymbol{x}_{k-N_1}-\boldsymbol{\xi}_j^{(1)}\right|\right)\\ \quad\times\dfrac{(\boldsymbol{x}_{k-N_1}-\boldsymbol{\xi}_j^{(1)})\cdot\mathbf{n}(\boldsymbol{x}_{k-N_1})}{|\boldsymbol{x}_{k-N_1}-\boldsymbol{\xi}_j^{(1)}|}, & j=\overline{1,N},\\ -\sqrt{\alpha_{\rm x}^{(2)}}K_1\left(\sqrt{\alpha_{\rm x}^{(2)}}\left|\boldsymbol{x}_{k-N_1}-\boldsymbol{\xi}_{j-N}^{(2)}\right|\right) & k=\overline{N_1+1,2N_1},\\ \quad\times\dfrac{\left(\boldsymbol{x}_{k-N_1}-\boldsymbol{\xi}_{j-N}^{(2)}\right)\cdot\mathbf{n}(\boldsymbol{x}_{k-N_1})}{|\boldsymbol{x}_{k-N_1}-\boldsymbol{\xi}_{j-N}^{(2)}|}, & j=\overline{N+1,N+M},\end{cases}\tag{3.8b}$$

$$A_{kj}=0,\quad j=\overline{1,N},\quad k=\overline{2N_1+1,2N_1+N_2},\tag{3.8c}$$

$$\begin{aligned}A_{kj}=&\frac{\mathcal{D}_{\rm x}\sqrt{\alpha_{\rm x}^{(2)}}}{\pi}K_1\left(\sqrt{\alpha_{\rm x}^{(2)}}\left|\boldsymbol{x}_{k-2N_1}-\boldsymbol{\xi}_{j-N}^{(2)}\right|\right)\frac{(\boldsymbol{x}_{k-2N_1}-\boldsymbol{\xi}_{j-N}^{(2)})\cdot\boldsymbol{n}(\boldsymbol{x}_{k-2N_1})}{|\boldsymbol{x}_{k-2N_1}-\boldsymbol{\xi}_{j-N}^{(2)}|}\\ &+\frac{\gamma}{2\pi}K_0\left(\sqrt{\alpha_{\rm x}^{(2)}}\left|\boldsymbol{x}_{k-2N_1}-\boldsymbol{\xi}_{j-N}^{(2)}\right|\right),\quad j=\overline{N+1,N+M},\\ &\qquad\qquad k=\overline{2N_1+1,2N_1+N_2}.\end{aligned}\tag{3.8d}$$

Linear system (3.6) could be under-determined, determined and over-determined, and these three scenarios were discussed in [27]. Herein, we consider only the determined and over-determined case with $2N_1+N_2\geq N+M$. Moreover, the MFS system (3.6) is ill-conditioned [26]. However, since the vector $\boldsymbol{c}$ contains fictitious unphysical coefficients their possibly large values resulting from the least-squares inversion $(A^{\rm T}A)^{-1}A^{\rm T}\boldsymbol{b}$ are not of great concern since, when introduced into the original MFS expansions (3.3) and (3.4), they yield accurate approximations of the physical solutions for $u^{(1)}$ and $u^{(2)}$, provided that the source points are suitably chosen [3]. In case of irregular boundary data and non-smooth domains, regularization of the system of equations may need to be employed [8].

3.2. The MFS for the emission fluence

The elimination of $u^{(1)}$ in (2.7a) and (2.7b) results in the fourth order PDE

$$\left(\Delta-\alpha_{\rm x}^{(1)}\mathcal{I}\right)\left(\Delta-\alpha_{\rm m}^{(1)}\mathcal{I}\right)v^{(1)}=0\quad\text{in D},\tag{3.9}$$

where $\mathcal{I}$ is the identity operator. Also, eliminating $u^{(2)}$ in (2.7a) and (2.7d) gives

$$\left(\Delta-\alpha_{\rm x}^{(2)}\mathcal{I}\right)\left(\Delta-\alpha_{\rm m}^{(2)}\mathcal{I}\right)v^{(2)}=0\quad\text{in }\Omega\backslash\overline{\rm D}.\tag{3.10}$$

Eliminating $u^{(2)}$ between (2.9a) and (2.7d) yields

$$2\mathcal{D}_{\rm x}\frac{\partial(\Delta v^{(2)}-\alpha_{\rm m}^{(2)}v^{(2)})}{\partial n}+\gamma\left(\Delta v^{(2)}-\alpha_{\rm m}^{(2)}v^{(2)}\right)=SB_{\rm x}^{(2)}\quad\text{on }\partial\Omega.\tag{3.11}$$

Also, using (2.7b), (2.7d), (2.8a) and (2.8c), we obtain the additional ICs

$$B_{\mathrm{x}}^{(1)}\Delta v^{(2)} - \alpha_{\mathrm{m}}^{(2)}B_{\mathrm{x}}^{(1)}v^{(2)} = B_{\mathrm{x}}^{(2)}\Delta v^{(1)} - \alpha_{\mathrm{m}}^{(1)}B_{\mathrm{x}}^{(2)}v^{(1)} \quad \text{on } \partial\mathrm{D}, \tag{3.12a}$$

$$B_{\mathrm{x}}^{(1)}\frac{\partial(\Delta v^{(2)})}{\partial \mathrm{n}} - \alpha_{\mathrm{m}}^{(2)}B_{\mathrm{x}}^{(1)}\frac{\partial v^{(2)}}{\partial \mathrm{n}} = B_{\mathrm{x}}^{(2)}\frac{\partial(\Delta v^{(1)})}{\partial \mathrm{n}} - \alpha_{\mathrm{m}}^{(1)}B_{\mathrm{x}}^{(2)}\frac{\partial v^{(1)}}{\partial \mathrm{n}} \quad \text{on } \partial\mathrm{D}. \tag{3.12b}$$

We shall therefore consider the BVP consisting of the PDEs (3.9) and (3.10), the ICs (2.8b), (2.8d), (3.12a) and (3.12b), and the BCs (2.9b) and (3.11).

In two dimensions, the fundamental solutions of (3.9) and (3.10) are given by [20]

$$V^{(\ell)}(\boldsymbol{x};\boldsymbol{\xi}) = -\frac{1}{2\pi(\alpha_{\mathrm{m}}^{(\ell)} - \alpha_{\mathrm{x}}^{(\ell)})} \times \left[K_0\left(\sqrt{\alpha_{\mathrm{m}}^{(\ell)}}|\boldsymbol{x}-\boldsymbol{\xi}|\right) - K_0\left(\sqrt{\alpha_{\mathrm{x}}^{(\ell)}}|\boldsymbol{x}-\boldsymbol{\xi}|\right)\right], \quad \ell = 1,2. \tag{3.13}$$

Then, we employ the MFS approximations

$$v^{(1)}(\boldsymbol{x}) \approx \tilde{v}^{(1)}(\boldsymbol{x}) = \sum_{j=1}^{2N} d_j^{(1)} V^{(1)}\big(\boldsymbol{x};\boldsymbol{\xi}_j^{(1)}\big), \quad \boldsymbol{x} \in \overline{\mathrm{D}}, \tag{3.14a}$$

$$v^{(2)}(\boldsymbol{x}) \approx \tilde{v}^{(2)}(\boldsymbol{x}) = \sum_{j=1}^{2M} d_j^{(2)} V^{(2)}\big(\boldsymbol{x};\boldsymbol{\xi}_j^{(2)}\big), \quad \boldsymbol{x} \in \overline{\Omega}\backslash\mathrm{D}, \tag{3.14b}$$

where $(\boldsymbol{\xi}_j^{(1)})_{j=\overline{1,N}}$ and $(\boldsymbol{\xi}_j^{(1)})_{j=\overline{N+1,2N}}$ are sources situated outside $\overline{\mathrm{D}}$ on two similar, closed, non-intersecting pseudo-boundaries [19], see also [9]. Similarly, $(\boldsymbol{\xi}_j^{(2)})_{j=\overline{1,M}}$ and $(\boldsymbol{\xi}_j^{(2)})_{j=\overline{M+1,2M}}$ are sources situated outside $\overline{\Omega}\backslash\mathrm{D}$, i.e. situated inside D and outside $\overline{\Omega}$ on four (two similar pairs), closed, non-intersecting pseudo-boundaries.

In the MFS expansions (3.14a) and (3.14b), the unknown complex coefficients $(d_j^{(1)})_{j=\overline{1,2N}}$ and $(d_j^{(2)})_{j=\overline{1,2M}}$ are determined by imposing the ICs (2.8b), (2.8d), (3.12a) and (3.12b), and the BCs (2.9b) and (3.11), at the boundary points $(\boldsymbol{x}_k)_{k=\overline{1,N_1}}$ $\in \partial\mathrm{D}$ and $(\boldsymbol{x}_k)_{k=\overline{N_1+1,N_1+N_2}} \in \partial\Omega$, respectively. This collocation process yields the following system of $4N_1 + 2N_2$ complex equations in $2N + 2M$ complex unknowns:

$$\mathrm{A}\mathbf{d} = \mathbf{b}, \quad \text{where} \quad \mathbf{d} = \left(\left(d_j^{(1)}\right)_{j=\overline{1,2N}}, \left(d_j^{(2)}\right)_{j=\overline{1,2M}}\right)^{\mathrm{T}}, \tag{3.15}$$

$$\mathrm{b}_k = \begin{cases} 0, & k = \overline{1, 4N_1 + N_2}, \\ B_{\mathrm{x}}^{(2)} S(\boldsymbol{x}_{k-(3N_1+N_2)}), & k = \overline{4N_1 + N_2 + 1, 4N_1 + 2N_2}, \end{cases} \tag{3.16}$$

$$\mathrm{A}_{kj} = \begin{cases} V^{(1)}\big(\boldsymbol{x}_k;\boldsymbol{\xi}_j^{(1)}\big), & j = \overline{1, 2N}, \\ -V^{(2)}\big(\boldsymbol{x}_k;\boldsymbol{\xi}_{j-2N}^{(2)}\big), & j = \overline{2N+1, 2N+2M}, \end{cases} \quad k = \overline{1, N_1}, \tag{3.17a}$$

$$\mathrm{A}_{kj} = \begin{cases} \dfrac{\partial V^{(1)}}{\partial \mathrm{n}}\big(\boldsymbol{x}_{k-N_1};\boldsymbol{\xi}_j^{(1)}\big), & j=\overline{1,2N}, \\ -\dfrac{\partial V^{(2)}}{\partial \mathrm{n}}\big(\boldsymbol{x}_{k-N_1};\boldsymbol{\xi}_{j-2N}^{(2)}\big), & j=\overline{2N+1,2N+2M}, \end{cases} \quad k=\overline{N_1+1,2N_1}, \tag{3.17b}$$

$$\mathrm{A}_{kj} = \begin{cases} B_{\mathrm{x}}^{(2)}\Delta V^{(1)}\big(\boldsymbol{x}_{k-2N_1};\boldsymbol{\xi}_j^{(1)}\big) \\ \quad -\alpha_{\mathrm{m}}^{(1)}B_{\mathrm{x}}^{(2)}V^{(1)}\big(\boldsymbol{x}_{k-2N_1};\boldsymbol{\xi}_j^{(1)}\big), & j=\overline{1,2N}, \\ -\Big(B_{\mathrm{x}}^{(1)}\Delta V^{(2)}\big(\boldsymbol{x}_{k-2N_1};\boldsymbol{\xi}_{j-2N}^{(2)}\big) \\ \quad -\alpha_{\mathrm{m}}^{(2)}B_{\mathrm{x}}^{(1)}V^{(2)}\big(\boldsymbol{x}_{k-2N_1};\boldsymbol{\xi}_{j-2N}^{(2)}\big)\Big), & j=\overline{2N+1,2N+2M}, \end{cases} \quad k=\overline{2N_1+1,3N_1}, \tag{3.17c}$$

$$\mathrm{A}_{kj} = \begin{cases} B_{\mathrm{x}}^{(2)}\dfrac{\partial(\Delta V^{(1)})}{\partial \mathrm{n}}\big(\boldsymbol{x}_{k-3N_1};\boldsymbol{\xi}_j^{(1)}\big) \\ \quad -\alpha_{\mathrm{m}}^{(1)}B_{\mathrm{x}}^{(2)}\dfrac{\partial V^{(1)}}{\partial \mathrm{n}}(\boldsymbol{x}_{k-3N_1};\boldsymbol{\xi}_j^{(1)}), & j=\overline{1,2N}, \\ -\Big(B_{\mathrm{x}}^{(1)}\dfrac{\partial(\Delta V^{(2)})}{\partial \mathrm{n}}\big(\boldsymbol{x}_{k-3N_1};\boldsymbol{\xi}_{j-2N}^{(2)}\big) \\ \quad -\alpha_{\mathrm{m}}^{(2)}B_{\mathrm{x}}^{(1)}\dfrac{\partial V^{(2)}}{\partial \mathrm{n}}\big(\boldsymbol{x}_{k-3N_1};\boldsymbol{\xi}_{j-2N}^{(2)}\big)\Big), & j=\overline{2N+1,2N+2M}, \end{cases} \quad k=\overline{3N_1+1,4N_1}, \tag{3.17d}$$

$$\mathrm{A}_{kj}=0, \quad j=\overline{1,2N}, \quad k=\overline{4N_1+1,4N_1+2N_2}, \tag{3.17e}$$

$$\begin{aligned} \mathrm{A}_{kj} &= 2\mathcal{D}_{\mathrm{m}}\frac{\partial V^{(2)}}{\partial n}\big(\boldsymbol{x}_{k-3N_1};\boldsymbol{\xi}_{j-2N}^{(2)}\big)+\gamma V^{(2)}\big(\boldsymbol{x}_{k-3N_1};\boldsymbol{\xi}_{j-2N}^{(2)}\big), \\ &\qquad j=\overline{2N+1,2N+2M}, \quad k=\overline{4N_1+1,4N_1+N_2}, \end{aligned} \tag{3.17f}$$

$$\begin{aligned} \mathrm{A}_{kj} &= 2\mathcal{D}_{\mathrm{x}}\frac{\partial(\Delta V^{(2)}-\alpha_{\mathrm{m}}^{(2)}V^{(2)})}{\partial n}\big(\boldsymbol{x}_{k-3N_1-N_2};\boldsymbol{\xi}_{j-2N}^{(2)}\big) \\ &\quad +\gamma\big(\Delta V^{(2)}-\alpha_{\mathrm{m}}^{(2)}V^{(2)}\big)\big(\boldsymbol{x}_{k-3N_1-N_2};\boldsymbol{\xi}_{j-2N}^{(2)}\big), \\ &\qquad j=\overline{2N+1,2N+2M}, \quad k=\overline{4N_1+N_2+1,4N_1+2N_2}. \end{aligned} \tag{3.17g}$$

As in Section 3.1, we consider the system of Eqs. (3.15) only in the determined or over-determined situation and therefore we require $2N_1+N_2 \geq N+M$.

3.3. Selection of sources and boundary collocation points

We consider numerical experiments for optical fluorescence in a circular plate of radius 4 cm such that upon dimensionalisation with the diameter L=8 cm of all distances (or lengths) involved, the non-dimensional domain

$$\Omega = \big\{(r,\vartheta)\,|\,0 \leq r < R = 1/2, \vartheta \in [0,2\pi)\big\}.$$

We assume that the defect $\mathrm{D} \subset \Omega$ is star-shaped with respect to the origin, parameter-

ized in polar coordinates by

$$\mathrm{D} = \big\{ r(\cos\vartheta, \sin\vartheta) | \vartheta \in [0, 2\pi), 0 \le r < r(\vartheta) \big\}, \tag{3.18}$$

where $r(\vartheta) < 1/2$ is a 2π-periodic smooth function.

In the MFS approximation (3.3) for $u^{(1)}$ in $\overline{\mathrm{D}}$, we take the source points

$$\xi_j^{(1)} = \delta r(\vartheta_j)\,(\cos\vartheta_j, \sin\vartheta_j)\,, \quad j = \overline{1, N}, \tag{3.19}$$

where $\delta > 1$ is a parameter to be prescribed and $\vartheta_j = 2\pi(j-1)/N$ for $j = \overline{1, N}$. Also, in the MFS approximation (3.4) for $u^{(2)}$ in $\overline{\Omega}\backslash\mathrm{D}$, we take the source points

$$\begin{aligned} \xi_j^{(2)} &= \delta_1 r(\tilde{\vartheta}_j)\big(\cos\tilde{\vartheta}_j, \sin\tilde{\vartheta}_j\big), \quad j = \overline{1, M_1}, \\ \xi_{M_1+j}^{(2)} &= \delta_2 R\big(\cos\hat{\vartheta}_j, \sin\hat{\vartheta}_j\big), \quad j = \overline{1, M_2}, \end{aligned} \tag{3.20}$$

where $1 > \delta_1 > 0, \delta_2 > 1$ are parameters to be prescribed and $\tilde{\vartheta}_j = 2\pi(j-1)/M_1$ for $j = \overline{1, M_1}$, $\hat{\vartheta}_j = 2\pi(j-1)/M_2$ for $j = \overline{1, M_2}$, and $M_1 + M_2 = M$. The source points (3.19) and (3.20) are shown in Fig. 2(a).

In the MFS approximation (3.14a) for $v^{(1)}$ in $\overline{\mathrm{D}}$, we take the additional source points

$$\xi_{N+j}^{(1)} = \eta r(\vartheta_j)\,(\cos\vartheta_j, \sin\vartheta_j)\,, \quad j = \overline{1, N}, \tag{3.21}$$

where $\eta > \delta > 1$. Also, in the MFS approximation (3.14b) for $v^{(2)}$ in $\overline{\Omega}\backslash\mathrm{D}$, we take the additional source points

$$\begin{aligned} \xi_{M+j}^{(2)} &= \eta_1 r(\tilde{\vartheta}_j)\big(\cos\tilde{\vartheta}_j, \sin\tilde{\vartheta}_j\big), \quad j = \overline{1, M_1}, \\ \xi_{M_1+M+j}^{(2)} &= \eta_2 R\big(\cos\hat{\vartheta}_j, \sin\hat{\vartheta}_j\big), \quad j = \overline{1, M_2}, \end{aligned} \tag{3.22}$$

where $1 > \delta_1 > \eta_1 > 0$ and $\eta_2 > \delta_2 > 1$. The source points (3.19)-(3.22) are illustrated in Fig. 2(b).

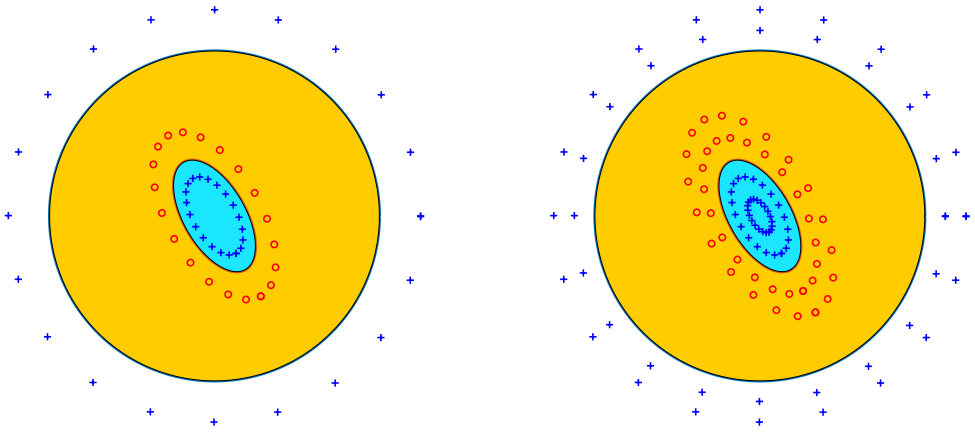

(a) Sources for $u^{(1)}, u^{(2)}$ (b) Sources for $v^{(1)}, v^{(2)}$

Figure 2: Source configurations for (a) $u^{(1)}, u^{(2)}$ and (b) $v^{(1)}, v^{(2)}$. The red sources o correspond to the domain D and the blue sources $+$ correspond to the domain $\Omega\backslash\overline{\mathrm{D}}$.

We also take the boundary collocation points

$$\boldsymbol{x}_k = \begin{cases} r(\overline{\theta}_k)\left(\cos\overline{\theta}_k, \sin\overline{\theta}_k\right) \in \partial\mathrm{D}, & k = \overline{1, N_1}, \\ R\big(\cos\overline{\overline{\theta}}_{k-N_1}, \sin\overline{\overline{\theta}}_{k-N_1}\big) \in \partial\Omega, & k = \overline{N_1+1, N_1+N_2}, \end{cases} \tag{3.23}$$

where $\overline{\theta}_k = 2\pi(k-1)/N_1$ for $k = \overline{1, N_1}$ and $\overline{\overline{\theta}}_k = 2\pi(k-1)/N_2$ for $k = \overline{1, N_2}$.

The inward normal $\mathbf{n}$ to the boundary

$$\partial\mathrm{D} = \left\{r(\vartheta)(\cos\vartheta, \sin\vartheta) | \vartheta \in [0, 2\pi)\right\}$$

of the star-shaped domain (3.18), which is needed in expressions (3.5b) is given by, see e.g. [21],

$$\begin{aligned} &\mathbf{n}(\boldsymbol{x}) = -\frac{1}{\sqrt{r^2(\theta) + r'^2(\theta)}}\left(r'(\theta)\sin\theta + r(\theta)\cos\theta, r(\theta)\sin\theta - r'(\theta)\cos\theta\right), \\ &\boldsymbol{x} = r(\theta)\left(\cos\theta, \sin\theta\right), \quad \theta \in [0, 2\pi). \end{aligned} \tag{3.24}$$

4. Numerical experiments

From previous medical phantom optical fluorescence imaging experiments [14–17, 20] we take the following physical parameters:

$$\begin{aligned} &\varphi = 0.016, \quad \tau = 0.56 \times 10^{-9}, \quad \omega = 10^8 \mathrm{s}^{-1}, \quad c = 3 \times 10^{10} \mathrm{cm/s}, \quad \gamma = 0.9566, \\ &\mu'_{\mathrm{sx}} = \mu'_{\mathrm{sm}} = 9.84\mathrm{cm}^{-1}, \quad \mu_{\mathrm{ami}} = 0.0289\mathrm{cm}^{-1}, \quad \mu_{\mathrm{axi}} = 0.023\mathrm{cm}^{-1}, \\ &\mu_{\mathrm{axf}}(\boldsymbol{x}) = \begin{cases} \mu^{(1)}_{\mathrm{axf}}(\boldsymbol{x}) = 0.5\mathrm{cm}^{-1}, & \boldsymbol{x} \in \mathrm{D}, \\ \mu^{(2)}_{\mathrm{axf}}(\boldsymbol{x}) = 0.005\mathrm{cm}^{-1}, & \boldsymbol{x} \in \Omega\backslash\overline{\mathrm{D}}, \end{cases} \\ &\mu_{\mathrm{amf}}(\boldsymbol{x}) = \begin{cases} \mu^{(1)}_{\mathrm{amf}}(\boldsymbol{x}) = 0.0506\mathrm{cm}^{-1}, & \boldsymbol{x} \in \mathrm{D}, \\ \mu^{(2)}_{\mathrm{amf}}(\boldsymbol{x}) = 0.00506\mathrm{cm}^{-1}, & \boldsymbol{x} \in \Omega\backslash\overline{\mathrm{D}}. \end{cases} \end{aligned}$$

Note that the coefficients characterising absorption due to exogenous fluorosphore at excitation and emission wavelength are 100 and 10 times, respectively, greater in the tumour domain D than in the surrounding healthy tissue $\Omega\backslash\overline{\mathrm{D}}$. The above data yield the following non-dimensional quantities:

$$\begin{aligned} &\alpha^{(1)}_{\mathrm{x}} = 1040.611008 + 6.632319999\mathrm{i}, && \alpha^{(2)}_{\mathrm{x}} = 53.050368 + 6.315519999\mathrm{i}, \\ &\alpha^{(1)}_{\mathrm{m}} = 151.411248 + 6.348479999\mathrm{i}, && \alpha^{(2)}_{\mathrm{m}} = 64.38137887 + 6.319334399\mathrm{i}, \\ &B^{(1)}_{\mathrm{x}} = 15.18872017 + 0.8505683298\mathrm{i}, && B^{(2)}_{\mathrm{x}} = 0.1511898941 + 0.00846663407\mathrm{i}, \\ &\mathcal{D}_{\mathrm{x}} = 0.004222402378, && \mathcal{D}_{\mathrm{m}} = 0.004219853702. \end{aligned}$$

We also take $\mathrm{D} \subset \Omega$ to be a circle of radius $r(\theta) = R_0 = 0.25$ for $\theta \in [0, 2\pi)$ centred at the origin. The MFS numerical parameters $N, N_1, N_2, M_1, M_2, \delta, \delta_1, \delta_2, \eta, \eta_1$ and η_2 are to be specified.

4.1. Example 1: Numerical verification for u

On solving the direct problem given by Eqs. (2.7a), (2.7c), (2.8a), (2.8c) and (2.9a) using the MFS, as described in Section 3.1, we obtain the solutions $u^{(1)}$ in D and $u^{(2)}$ in $\Omega\backslash\overline{\mathrm{D}}$. To verify the code we take the analytical solution for u in Ω given by

$$u(r,\vartheta)=\begin{cases}u^{(1)}(r,\vartheta)=I_0\big(\beta_{\mathrm{x}}^{(1)}r\big), & (r,\vartheta)\in \mathrm{D},\\ u^{(2)}(r,\vartheta)=AI_0\big(\beta_{\mathrm{x}}^{(2)}r\big)+BK_0\big(\beta_{\mathrm{x}}^{(2)}r\big), & (r,\vartheta)\in \Omega\backslash\overline{\mathrm{D}},\end{cases} \tag{4.1}$$

where $\beta_{\mathrm{x}}^{(\ell)}:=\sqrt{\alpha_{\mathrm{x}}^{(\ell)}}$ for $\ell=1,2$,

$$A=\frac{I_0(\beta_{\mathrm{x}}^{(1)}R_0)K_1(\beta_{\mathrm{x}}^{(2)}R_0)+(\beta_{\mathrm{x}}^{(1)}/\beta_{\mathrm{x}}^{(2)})I_1(\beta_{\mathrm{x}}^{(1)}R_0)K_0(\beta_{\mathrm{x}}^{(2)}R_0)}{I_0(\beta_{\mathrm{x}}^{(2)}R_0)K_1(\beta_{\mathrm{x}}^{(2)}R_0)+I_1(\beta_{\mathrm{x}}^{(2)}R_0)K_0(\beta_{\mathrm{x}}^{(2)}R_0)}, \tag{4.2}$$

$$B=\frac{I_0(\beta_{\mathrm{x}}^{(1)}R_0)I_1(\beta_{\mathrm{x}}^{(2)}R_0)-(\beta_{\mathrm{x}}^{(1)}/\beta_{\mathrm{x}}^{(2)})I_0(\beta_{\mathrm{x}}^{(2)}R_0)I_1(\beta_{\mathrm{x}}^{(1)}R_0)}{I_0(\beta_{\mathrm{x}}^{(2)}R_0)K_1(\beta_{\mathrm{x}}^{(2)}R_0)+I_1(\beta_{\mathrm{x}}^{(2)}R_0)K_0(\beta_{\mathrm{x}}^{(2)}R_0)}, \tag{4.3}$$

where I_ℓ and K_ℓ are modified Bessel functions of order $\ell\in\{0,1\}$ of the first and second kind, respectively. The function S on $\partial\Omega$ can be fabricated from Eqs. (2.9a) and (4.1) for $u^{(2)}$ as

$$\begin{aligned}S(R,\vartheta)=-\gamma u^{(2)}(R,\vartheta)-2\mathcal{D}_{\mathrm{x}}\frac{\partial u^{(2)}}{\partial r}(R,\vartheta)=-\gamma\left(AI_0(\beta_{\mathrm{x}}^{(2)}R)+BK_0(\beta_{\mathrm{x}}^{(2)}R)\right)\\ -2\mathcal{D}_{\mathrm{x}}\beta_{\mathrm{x}}^{(2)}\left(AI_1(\beta_{\mathrm{x}}^{(2)}R)-BK_1(\beta_{\mathrm{x}}^{(2)}R)\right)=\text{constant},\quad \vartheta\in[0,2\pi).\end{aligned}$$

4.2. Example 2: Numerical verification for v

Also, on solving the direct problem given by Eqs. (3.9), (3.10), (2.8b), (2.8d), (3.12a), (2.9b), (3.11) and (3.12b) by the MFS as described in Section 3.2, we obtain the solutions $v^{(1)}$ in D and $v^{(2)}$ in $\Omega\backslash\overline{\mathrm{D}}$. To verify the code in this case we take the analytical solution for v in Ω given by

$$v(r,\vartheta)=\begin{cases}v^{(1)}(r,\vartheta)=\dfrac{B_{\mathrm{x}}^{(1)}}{\alpha_{\mathrm{x}}^{(1)}-\alpha_{\mathrm{m}}^{(1)}}\left[I_0(\beta_{\mathrm{m}}^{(1)}r)-I_0(\beta_{\mathrm{x}}^{(1)}r)\right], & (r,\vartheta)\in \mathrm{D},\\ v^{(2)}(r,\vartheta)=\dfrac{B_{\mathrm{x}}^{(2)}}{\alpha_{\mathrm{x}}^{(2)}-\alpha_{\mathrm{m}}^{(2)}}\Big[A\left[I_0(\beta_{\mathrm{m}}^{(2)}r)-I_0(\beta_{\mathrm{x}}^{(2)}r)\right]\\ \qquad\qquad +B\left[K_0(\beta_{\mathrm{m}}^{(2)}r)-K_0(\beta_{\mathrm{x}}^{(2)}r)\right]\\ \qquad\qquad +CI_0(\beta_{\mathrm{m}}^{(2)}r)+DK_0(\beta_{\mathrm{m}}^{(2)}r)\Big], & (r,\vartheta)\in \Omega\backslash\overline{\mathrm{D}},\end{cases} \tag{4.4}$$

where $\beta_{\rm m}^{(\ell)} := \sqrt{\alpha_{\rm m}^{(\ell)}}$ for $\ell = 1, 2$, and

$$C = -A + Z\frac{[I_0(\beta_{\rm m}^{(1)}R_0)K_1(\beta_{\rm m}^{(2)}R_0) + (\beta_{\rm m}^{(1)}/\beta_{\rm m}^{(2)})I_1(\beta_{\rm m}^{(1)}R_0)K_0(\beta_{\rm m}^{(2)}R_0)]}{I_0(\beta_{\rm m}^{(2)}R_0)K_1(\beta_{\rm m}^{(2)}R_0) + I_1(\beta_{\rm m}^{(2)}R_0)K_0(\beta_{\rm m}^{(2)}R_0)}$$
$$+ (1-Z)\frac{[I_0(\beta_{\rm x}^{(1)}R_0)K_1(\beta_{\rm m}^{(2)}R_0) + (\beta_{\rm x}^{(1)}/\beta_{\rm m}^{(2)})I_1(\beta_{\rm x}^{(1)}R_0)K_0(\beta_{\rm m}^{(2)}R_0)]}{I_0(\beta_{\rm m}^{(2)}R_0)K_1(\beta_{\rm m}^{(2)}R_0) + I_1(\beta_{\rm m}^{(2)}R_0)K_0(\beta_{\rm m}^{(2)}R_0)}, \tag{4.5}$$

$$D = -B + Z\frac{[I_0(\beta_{\rm m}^{(1)}R_0)I_1(\beta_{\rm m}^{(2)}R_0) - (\beta_{\rm m}^{(1)}/\beta_{\rm m}^{(2)})I_0(\beta_{\rm m}^{(2)}R_0)I_1(\beta_{\rm m}^{(1)}R_0)]}{I_0(\beta_{\rm m}^{(2)}R_0)K_1(\beta_{\rm m}^{(2)}R_0) + I_1(\beta_{\rm m}^{(2)}R_0)K_0(\beta_{\rm m}^{(2)}R_0)}$$
$$+ (1-Z)\frac{[I_0(\beta_{\rm x}^{(1)}R_0)I_1(\beta_{\rm m}^{(2)}R_0) - (\beta_{\rm x}^{(1)}/\beta_{\rm m}^{(2)})I_0(\beta_{\rm m}^{(2)}R_0)I_1(\beta_{\rm x}^{(1)}R_0)]}{I_0(\beta_{\rm m}^{(2)}R_0)K_1(\beta_{\rm m}^{(2)}R_0) + I_1(\beta_{\rm m}^{(2)}R_0)K_0(\beta_{\rm m}^{(2)}R_0)}, \tag{4.6}$$

$$Z = \left(\frac{B_{\rm x}^{(1)}}{B_{\rm x}^{(2)}}\right)\left(\frac{\alpha_{\rm x}^{(2)} - \alpha_{\rm m}^{(2)}}{\alpha_{\rm x}^{(1)} - \alpha_{\rm m}^{(1)}}\right). \tag{4.7}$$

The above expressions have been verified using the MAPLE™ symbolic computation package.

Note that in place of (2.9b) we have satisfied its inhomogeneous form given by

$$\begin{aligned} 2\mathcal{D}_{\rm m}\frac{\partial v^{(2)}}{\partial n} + \gamma v^{(2)} &= \frac{2\mathcal{D}_{\rm m}B_{\rm x}^{(2)}}{\alpha_{\rm x}^{(2)} - \alpha_{\rm m}^{(2)}}\Bigg[A\left[\beta_{\rm m}^{(2)}I_1(\beta_{\rm m}^{(2)}R) - \beta_{\rm x}^{(2)}I_1(\beta_{\rm x}^{(2)}R)\right] \\ &\qquad + B\left[\beta_{\rm x}^{(2)}K_1(\beta_{\rm x}^{(2)}R) - \beta_{\rm m}^{(2)}K_1(\beta_{\rm m}^{(2)}R)\right] \\ &\qquad + C\beta_{\rm m}^{(2)}I_1(\beta_{\rm m}^{(2)}R) - D\beta_{\rm m}^{(2)}K_1(\beta_{\rm m}^{(2)}R)\Bigg] \\ &\quad + \frac{\gamma B_{\rm x}^{(2)}}{\alpha_{\rm x}^{(2)} - \alpha_{\rm m}^{(2)}}\Bigg[A\left[I_0(\beta_{\rm m}^{(2)}R) - I_0(\beta_{\rm x}^{(2)}R)\right] \\ &\qquad + B\left[K_0(\beta_{\rm m}^{(2)}R) - K_0(\beta_{\rm x}^{(2)}R)\right] \\ &\qquad + CI_0(\beta_{\rm m}^{(2)}R) + DK_0(\beta_{\rm m}^{(2)}R)\Bigg] \\ &=: {\rm R}_1(\vartheta), \quad \vartheta \in [0, 2\pi), \end{aligned} \tag{4.8}$$

and we impose (3.11) as

$$\begin{aligned} &2\mathcal{D}_{\rm x}\frac{\partial(\Delta v^{(2)} - \alpha_{\rm m}^{(2)}v^{(2)})}{\partial n} + \gamma\left(\Delta v^{(2)} - \alpha_{\rm m}^{(2)}v^{(2)}\right) \\ &= -2B_{\rm x}^{(2)}\beta_{\rm x}^{(2)}\mathcal{D}_{\rm x}\left(AI_1(\beta_{\rm x}^{(2)}R) - BK_1(\beta_{\rm x}^{(2)}R)\right) \\ &\quad - \gamma B_{\rm x}^{(2)}\left(AI_0(\beta_{\rm x}^{(2)}R) + BK_0(\beta_{\rm x}^{(2)}R)\right) \\ &=: {\rm R}_2(\vartheta), \quad \vartheta \in [0, 2\pi), \end{aligned} \tag{4.9}$$

where $S = {\rm R}_2/B_{\rm x}^{(2)}$.

In Table 1 we present the maximum relative errors $E_u^{(1)}$, $E_u^{(2)}$, $E_v^{(1)}$ and $E_v^{(2)}$ in $u^{(1)}$, $u^{(2)}$, $v^{(1)}$, $v^{(2)}$, respectively, calculated at 80 equally spaced points on the circles with radii $3/16$ in D and $3/8$ in $\Omega\backslash$D, respectively, for $\delta = 1.6$, $\delta_1 = 0.8$, $\delta_2 = 1.4$, $\eta = 2.2$, $\eta_1 = 0.6$, $\eta_2 = 2$, and five sets of increasing numbers of degrees of freedom denoted by $\mathrm{A}_1 - \mathrm{A}_6$. Clearly, we observe rapid convergence with increasing numbers of degrees of freedom. In Figs. 3 and 4 we present the plots of the converging real and imaginary parts of $u^{(2)}$ and $v^{(2)}$ on $\partial\Omega$, respectively, for the six different sets A_1-A_6 of Table 1.

Table 1: Example 1: Results for $E_u^{(1)}$, $E_u^{(2)}$, $E_v^{(1)}$ and $E_v^{(2)}$ for $\delta = 1.6$, $\delta_1 = 0.8$, $\delta_2 = 1.4$, $\eta = 2.2$, $\eta_1 = 0.6$, $\eta_2 = 2$.

Set	N_1	N_2	N	M_1	M_2	$E_u^{(1)}$	$E_u^{(2)}$	$E_v^{(1)}$	$E_v^{(2)}$
A_1	20	40	15	25	25	2.2235(-2)	4.4292(-4)	8.4762(-1)	4.2671(-3)
A_2	40	80	30	60	60	2.5110(-2)	9.5095(-4)	2.2374(-3)	1.7516(-5)
A_3	60	100	35	65	65	1.5083(-7)	6.4595(-9)	1.2005(-5)	6.3391(-8)
A_4	80	120	40	80	80	1.3733(-8)	9.2447(-10)	3.4917(-6)	3.1072(-8)
A_5	80	120	50	90	90	1.1781(-10)	2.3754(-12)	1.2222(-6)	3.8198(-9)
A_6	90	140	70	100	100	1.2786(-11)	2.5261(-13)	5.3284(-8)	1.5052(-10)

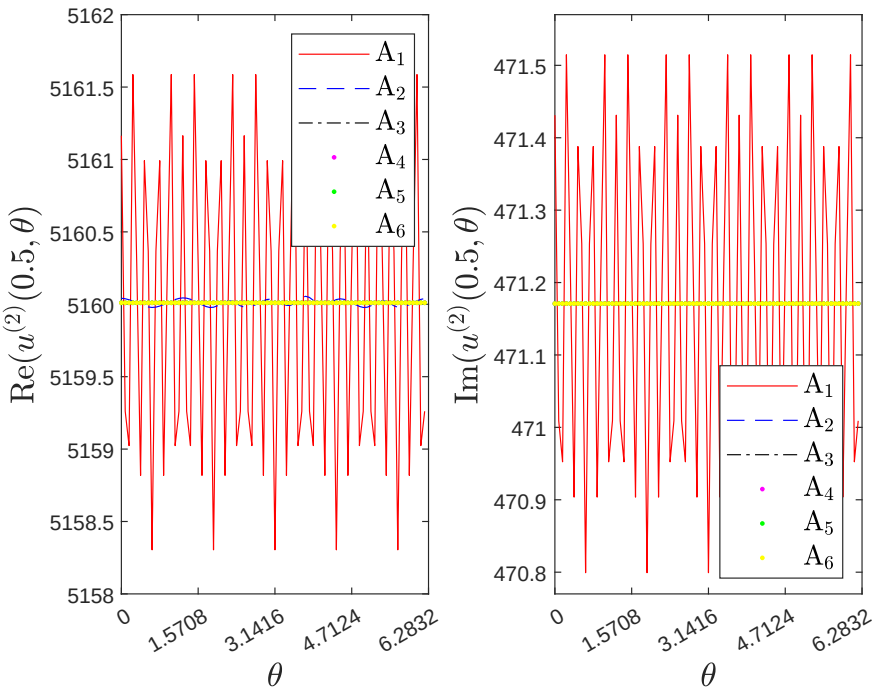

Figure 3: Convergence of the MFS real and imaginary parts of $u^{(2)}$ on $\partial\Omega$, as M and N increase, towards the exact values of $\mathrm{Re}(u^{(2)}(0.5,\theta) = 5160.010033861449$ and $\mathrm{Im}(u^{(2)}(0.5,\theta) = 471.170916239928$.

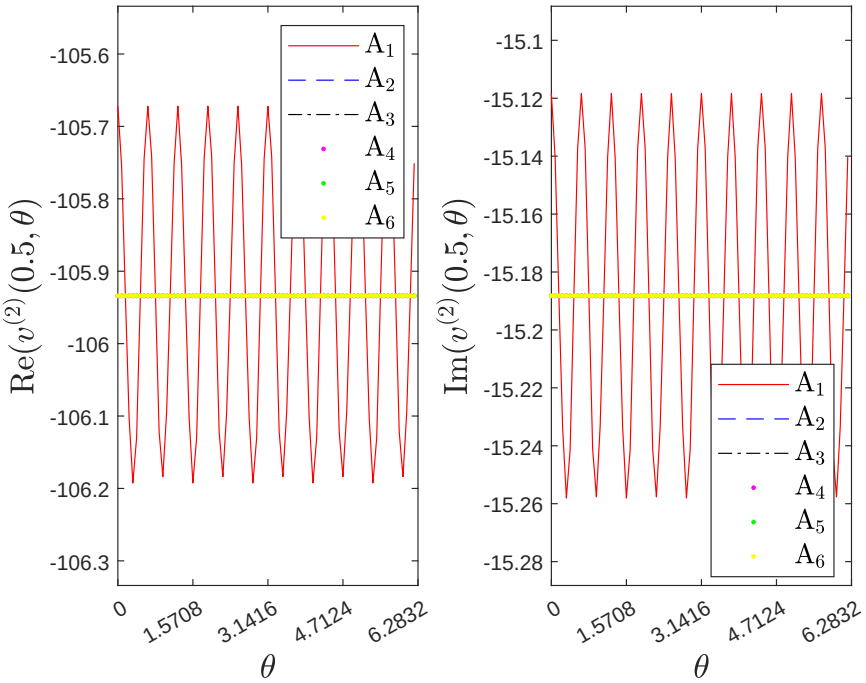

Figure 4: Convergence of the MFS real and imaginary parts of $v^{(2)}$ on $\partial\Omega$, as M and N increase, towards the exact values of $\mathrm{Re}(v^{(2)}(0.5,\theta) = -105.9340179530337$ and $\mathrm{Im}(v^{(2)}(0.5,\theta) = -15.1882374333592$.

5. The inverse problem

The usual inverse problem of optical fluorescence requires finding the dye-induced absorption coefficient $\mu_{\mathrm{axf}}(\boldsymbol{x})$ for $\boldsymbol{x} \in \Omega$ from the measurement of the complex-valued emission fluence v on a portion Γ of the boundary $\partial\Omega$, namely,

$$v = v^{(2)} = v^{(2)}_{\mathrm{measured}} \quad \text{on } \Gamma. \tag{5.1}$$

The coefficient μ_{axf} satisfies the physical constraint $0 < q_0 \leq \mu_{\mathrm{axf}}(\boldsymbol{x}) \leq q_1 < \infty$ for $\boldsymbol{x} \in \Omega$, where q_0 and q_1 are prescribed upper and lower bounds, respectively, that can inferred from physiological considerations [1]. We assume that the absorption coefficients μ_{axf} and μ_{amf} due to the exogenous fluorophore at excitation and emission wavelengths, respectively, are piecewise constant and given by (2.6). Under this assumption the goal of the inverse problem recasts as that of determining the anomaly D from the measurement (5.1). We assume that $\Omega\backslash\mathrm{D}$ is connected, though D may consist of several pieces of disjoint domains which are compactly contained in the host medium Ω. We also assume that D is star-shaped as given by (3.18) such that its boundary

$$\partial\mathrm{D} = \left\{r(\vartheta)(\cos\vartheta, \sin\vartheta) | \vartheta \in [0, 2\pi)\right\}, \tag{5.2}$$

where $0 < r(\vartheta) < 1/2$, is a 2π-periodic smooth unknown function.

If one were able to measure the complex-valued excitation fluence

$$u = u^{(2)} = u^{(2)}_{\text{measured}} \quad \text{on } \Gamma, \tag{5.3}$$

instead of (5.1), then the resulting inverse transmission problem for u (or $u^{(1)}$ and $u^{(2)}$) given by Eqs. (2.7a), (2.7c), (2.8a), (2.8c), (2.9a) and (5.3), which also arises in the determination of the contact resistivity of planar electronic devices [7], can be studied separately from that for v to search for the unknown anomaly D. This can be solved numerically using the MFS, as described in [6], or the boundary element method (BEM), as described in [25] in case $\alpha_{\mathrm{x}}^{(2)} = 0$. Furthermore, in case $\alpha_{\mathrm{x}}^{(2)} = 0$, uniqueness in determining the inhomogeneity D entering the inverse problem was established in the class of balls [18], star-shaped domains [12], convex hulls of polygons [24] and other classes of subdomains [23]. In practice, however, it is v that is measured as in (5.1), and this requires solving the inverse problem given by Eqs. (3.9), (3.10), (2.8b), (2.8d), (3.12a), (3.12b), (2.9b), (3.11) and (5.1).

5.1. Implementation

In the MFS formulation for the solution of inverse problem we place N_1 collocation points on $\partial\mathrm{D}$, N_2 collocation points on $\partial\Omega$, as well as N_3 collocation points on $\Gamma \subset \partial\Omega$. We also place $2N$ sources on the two pseudo-boundaries corresponding to $v^{(1)}$ in domain D, see Fig. 2(b), with $N = N_1$. Note that the radial values $r(\overline{\theta}_k) = r_k, k = \overline{1, N_1}$ in (3.23), are now unknown. For approximating the derivative $r'(\overline{\theta}_k)$ in (3.24) we use the central finite-difference

$$r'(\overline{\theta}_k) \approx \frac{r(\overline{\theta}_{k+1}) - r(\overline{\theta}_{k-1})}{4\pi/N_1}, \quad k = \overline{1, N_1} \tag{5.4}$$

with the convention that $\overline{\theta}_{N_1+1} = \overline{\theta}_1$ and $\overline{\theta}_{N_1} = \overline{\theta}_0$. For the domain $\Omega\backslash\mathrm{D}$ of $v^{(2)}$, we place $2M_1$ sources on two pseudo-boundaries inside D, with $M_1 = N_1$, and $2M_2$ sources on two pseudo-boundaries outside Ω, see Fig. 2(b). This means that we have the following unknowns:

- The $2N_1$ complex coefficients $\boldsymbol{d}^{(1)} = (d_j^{(1)})_{k=\overline{1,2N_1}}$ in (3.14a).
- The $2N_1 + 2M_2$ complex coefficients $\boldsymbol{d}^{(2)} = (d_j^{(2)})_{k=\overline{1,2N_1+2M_1}}$ in (3.14b).
- The (real) radii $\boldsymbol{r} = (r_k)_{k=\overline{1,N_1}}$ in (3.23).

The unknowns listed above are determined from the imposition of the BCs (2.9b), (3.11) and (5.1), and the ICs (2.8b), (2.8d), (3.12a), (3.12b) in a least-squares sense, which leads to minimizing the functional

$$S(\boldsymbol{d}^{(1)}, \boldsymbol{d}^{(2)}, \boldsymbol{r}) := \sum_{j=N_1+1}^{N_1+N_2} \left| 2\mathcal{D}_{\mathrm{m}} \frac{\partial \tilde{v}^{(2)}}{\partial n}(\boldsymbol{x}_j) + \gamma \tilde{v}^{(2)}(\boldsymbol{x}_j) \right|^2$$

$$
\begin{aligned}
&+\sum_{j=N_1+1}^{N_1+N_2}\left|2\mathcal{D}_{\mathrm{x}}\frac{\partial(\Delta\tilde{v}^{(2)}-\alpha_{\mathrm{m}}^{(2)}\tilde{v}^{(2)})}{\partial n}(\boldsymbol{x}_j)+\gamma\left(\Delta\tilde{v}^{(2)}(\boldsymbol{x}_j)-\alpha_{\mathrm{m}}^{(2)}\tilde{v}^{(2)}(\boldsymbol{x}_j)\right)-SB_{\mathrm{x}}^{(2)}\right|^2\\
&+\sum_{j=N_1+1}^{N_1+N_3}\left|\tilde{v}^{(2)}(\boldsymbol{x}_j)-v^{(2)}_{\mathrm{measured}(\varepsilon)}(\boldsymbol{x}_j)\right|^2\\
&+\sum_{j=1}^{N_1}\left|\tilde{v}^{(1)}(\boldsymbol{x}_j)-\tilde{v}^{(2)}(\boldsymbol{x}_j)\right|^2+\sum_{j=1}^{N_1}\left|\frac{\partial\tilde{v}^{(1)}}{\partial\mathrm{n}}(\boldsymbol{x}_j)-\frac{\partial\tilde{v}^{(2)}}{\partial\mathrm{n}}(\boldsymbol{x}_j)\right|^2\\
&+\sum_{j=1}^{N_1}\left|B_{\mathrm{x}}^{(1)}\Delta\tilde{v}^{(2)}(\boldsymbol{x}_j)-\alpha_{\mathrm{m}}^{(2)}B_{\mathrm{x}}^{(1)}\tilde{v}^{(2)}(\boldsymbol{x}_j)-\left(B_{\mathrm{x}}^{(2)}\Delta\tilde{v}^{(1)}(\boldsymbol{x}_j)-\alpha_{\mathrm{m}}^{(1)}B_{\mathrm{x}}^{(2)}\tilde{v}^{(1)}(\boldsymbol{x}_j)\right)\right|^2\\
&+\sum_{j=1}^{N_1}\left|B_{\mathrm{x}}^{(1)}\frac{\partial(\Delta\tilde{v}^{(2)})}{\partial\mathrm{n}}(\boldsymbol{x}_j)-\alpha_{\mathrm{m}}^{(2)}B_{\mathrm{x}}^{(1)}\frac{\partial\tilde{v}^{(2)}}{\partial\mathrm{n}}(\boldsymbol{x}_j)\right.\\
&\qquad\left.-\left(B_{\mathrm{x}}^{(2)}\frac{\partial(\Delta\tilde{v}^{(1)})}{\partial\mathrm{n}}(\boldsymbol{x}_j)-\alpha_{\mathrm{m}}^{(1)}B_{\mathrm{x}}^{(2)}\frac{\partial\tilde{v}^{(1)}}{\partial\mathrm{n}}(\boldsymbol{x}_j)\right)\right|^2\\
&+\lambda_1\left(|\boldsymbol{d}^{(1)}|^2+|\boldsymbol{d}^{(2)}|^2\right)+\lambda_2\sum_{\ell=2}^{N_1}(r_\ell-r_{\ell-1})^2,
\end{aligned}
\tag{5.5}
$$

where λ_1 and $\lambda_2\geq 0$ are regularization parameters that need to be prescribed and

$$
v^{(2)}_{\mathrm{measured}(\varepsilon)}(\boldsymbol{x}_j)=(1+\rho_j p)\,v^{(2)}_{\mathrm{measured}}(\boldsymbol{x}_j),\quad j=\overline{N_1+1,N_1+N_3},
\tag{5.6}
$$

where p represents the percentage of noise added to the boundary data on Γ and ρ_j is a pseudo-random noisy variable drawn from a uniform distribution in $[-1,1]$ using the MATLAB® command `-1+2*rand(1,`N_3`)`. Note that in (5.5), $|\cdot|$ represents the modulus of a complex number. The regularization terms

$$
\lambda_1\left(|\boldsymbol{d}^{(1)}|^2+|\boldsymbol{d}^{(2)}|^2\right)\quad\text{and}\quad\lambda_2\sum_{\ell=2}^{N_1}(r_\ell-r_{\ell-1})^2
$$

have been added to the functional (5.5) to stabilize the MFS solutions $\tilde{v}^\ell$, $\ell=1,2$, and the $\mathcal{C}^1$-smooth boundary $\partial\mathrm{D}$. Note that in (5.5) we have $9N_1+4M_2$ real unknowns and $8N_1+4N_2+2N_3$ boundary collocation equations so we need to take

$$
4N_2+2N_3\geq N_1+4M_2.
$$

5.2. Numerical results for the inverse problem

We considered the inverse problem for Example 2, which possesses the exact solution (4.4). More specifically, we examined the inverse BVP consisting of PDEs (3.9) and (3.10), BCs (2.9b), (3.11) and (5.1) (with $\Gamma=\partial\Omega$), and ICs (2.8b), (2.8d),

(3.12a) and (3.12b). The boundary $\partial\mathrm{D}$ of the inclusion D is unknown and is determined as the curve on which the ICs (2.8b), (2.8d), (3.12a) and (3.12b) are satisfied. We took $N_1 = M_1 = N_3 = 21$, $N_2 = 25$, $M_2 = 20$, $\delta = 1.25$, $\delta_1 = 0.8$, $\delta_2 = 1.5$, $\eta = 1.75$, $\eta_1 = 0.4$ and $\eta_2 = 2$. Moreover, we took the initial values of the MFS coefficients $\boldsymbol{d}^{(1)^{(0)}} = \mathbf{0}$, $\boldsymbol{d}^{(2)^{(0)}} = \mathbf{0}$ and the initial values of the radii $\boldsymbol{r}^{(0)} = \mathbf{0.375}$. The minimization of functional (5.5) was carried out using the MATLAB® routine `lsqnonlin`. In it, the user has the option of imposing lower and upper bounds on the elements of the vector of unknowns $\mathrm{Re}\{\boldsymbol{d}^{(1)}\}$, $\mathrm{Im}\{\boldsymbol{d}^{(1)}\}$, $\mathrm{Re}\{\boldsymbol{d}^{(2)}\}$, $\mathrm{Im}\{\boldsymbol{d}^{(2)}\}$ and $\boldsymbol{r}$ through the use of specified vectors $\mathbf{lb}$ and $\mathbf{up}$. In our applications, we imposed the constraints $-\mathbf{L} < \mathrm{Re}\{\boldsymbol{d}^{(1)}\}, \mathrm{Im}\{\boldsymbol{d}^{(1)}\} < \mathbf{U}$ and $-\mathbf{L} < \mathrm{Re}\{\boldsymbol{d}^{(2)}\}, \mathrm{Im}\{\boldsymbol{d}^{(2)}\} < \mathbf{U}$, where $\mathbf{L} = \mathbf{U} = 5 \times \mathbf{10^5}$ (with the appropriate dimensions since $\boldsymbol{d}^{(1)}$ and $\boldsymbol{d}^{(2)}$ have different dimensions). Further details regarding the implementation of `lsqnonlin` maybe found in [22]. Note that the first sum in (5.5) is replaced by (cf. (4.8))

$$\sum_{j=N_1+1}^{N_1+N_2} \left| 2\mathcal{D}_{\mathrm{m}} \frac{\partial \tilde{v}^{(2)}}{\partial n}(\boldsymbol{x}_j) + \gamma \tilde{v}^{(2)}(\boldsymbol{x}_j) - \mathrm{R}_1 \right|^2$$

and in the second sum, $SB_{\mathrm{x}}^{(2)}$ is replaced by R_2 (cf. (4.9)).

We first examined the case of no noise, i.e., $p = 0$ in (5.6), and found that the solution of the inverse BVP was highly challenging and unstable due to the presence of high derivatives in the BCs and, in particular, the ICs. We found it necessary to impose regularization to this problem with $\lambda_2 = 1$. In Fig. 5 we present the results obtained for different numbers of iterations `niter`, with no noise and regularization with $\lambda_2 = 1$, $\lambda_1 = 0$. It can be seen that the solution becomes accurate after about 1000 iterations.

In Figs. 6 and 7 we present the reconstructed curves for the noise level of $p = 5\%$ after 500 iterations and various regularization parameters λ_1 when $\lambda_2 = 0$, and λ_2 when $\lambda_1 = 0$, respectively. From these figures it can be seen that the inclusion of regularization with λ_2 yields stable numerical solutions. Finally, for completeness, in Fig. 8 we present the reconstructed curves for noise level of 5% after 500 iterations with both λ_1 and λ_2 regularization.

6. Conclusions

The MFS recently developed in [20] has been extended to deal with optical fluorescence direct BVPs in bi-layer materials. Numerical tests revealed the high accuracy of the proposed technique for the solution of such complicated problems. Furthermore, the MFS in combination with an iterative regularization constrained minimization technique, has been successfully applied to the numerical solution of nonlinear and ill-posed inverse geometric OFT problems. The versatility and ease of implementation of the meshless MFS offers further advantages over boundary and domain discretisation methods for potentially solving more challenging nonlinear inverse geometric problems in three dimensions.

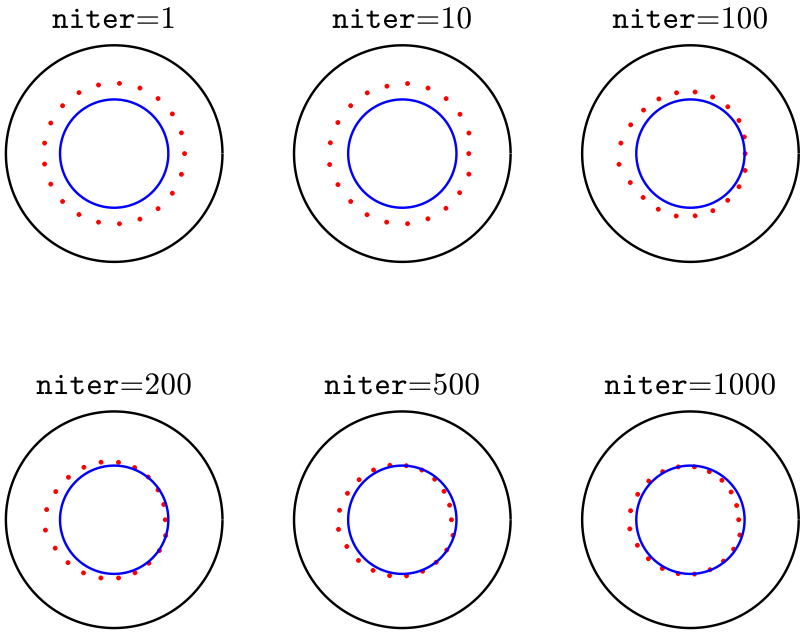

Figure 5: Inverse problem: Results for various numbers of iterations with no noise. The points of the reconstructed boundary are the red crosses $+$ and the exact boundary ∂D is the blue circle.

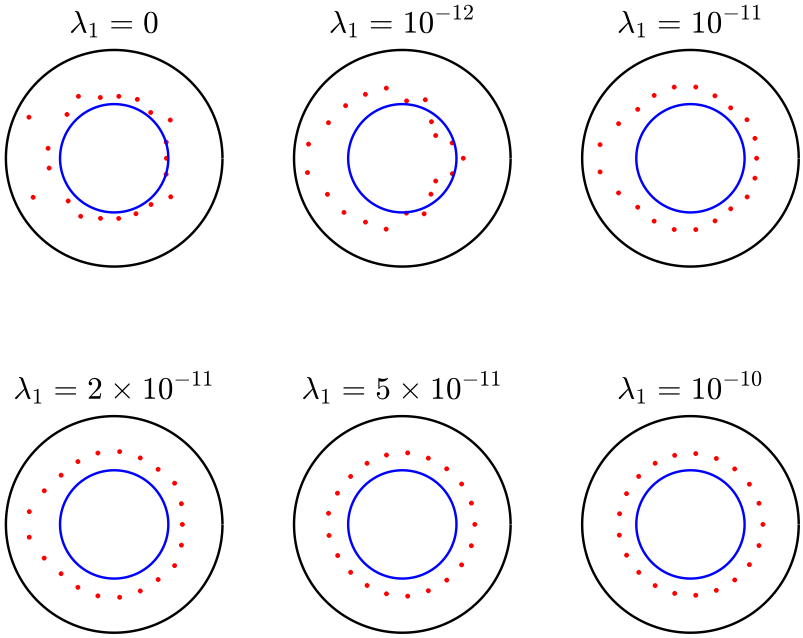

Figure 6: Inverse problem: Results for noise $p = 5\%$ and regularization with λ_1.

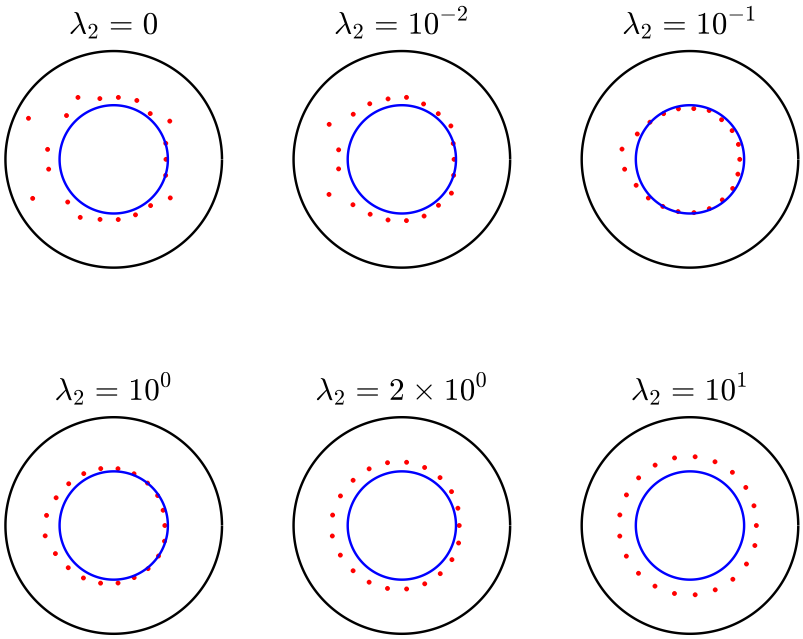

Figure 7: Inverse problem: Results for noise $p = 5\%$ and regularization with λ_2.

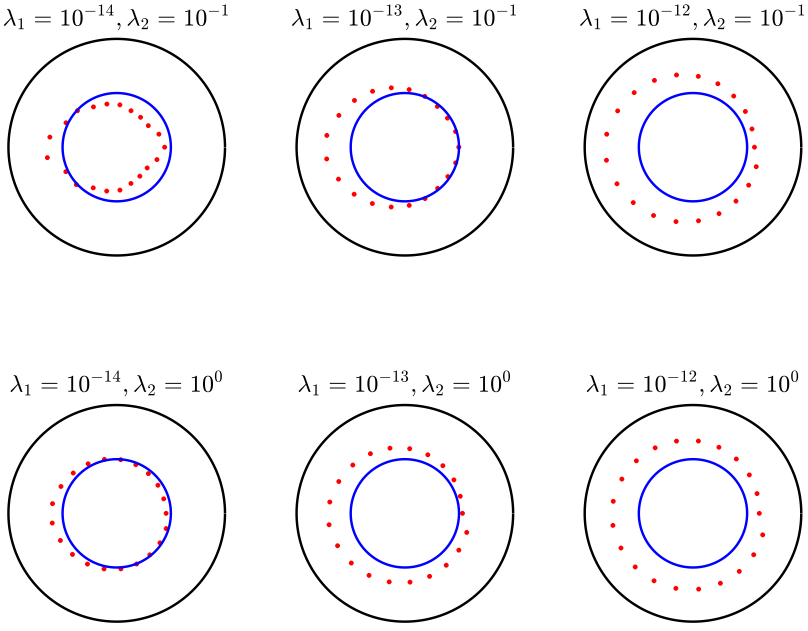

Figure 8: Inverse problem: Results for noise $p = 5\%$ and regularization with both λ_1 and λ_2.

Acknowledgments

Fruitful discussions with A. Joshi on the subject of fluorescence optical tomography are gratefully acknowledged.

References

[1] W. Bangerth, *A framework for the adaptive finite element solution of large inverse problems*, SIAM J. Sci. Comput. 30 (2008), 2965–2989.

[2] W. Bangerth and A. Joshi, *Adaptive finite element tomography for fluorescence optical imaging of tissue*, Inverse Probl. 24 (2008), Article ID 034011.

[3] A. H. Barnett and T. Betcke, *Stability and convergence of the method of fundamental solutions for Helmholtz problems on analytic domains*, J. Comput. Phys. 227 (2008), 7003–7026.

[4] J. R. Berger and A. Karageorghis, *The method of fundamental solutions for heat conduction in layered materials*, Int. J. Numer. Methods Eng. 45 (1999), 1681–1694.

[5] B. Bin-Mohsin and D. Lesnic, *The MFS for Helmholtz-type equations in layered materials*, in: Proceedings of the 8th UK Conference on Boundary Integral Methods, D. Lesnic (Ed), Leeds University Press, (2011), 57–64.

[6] B. Bin-Mohsin and D. Lesnic, *Numerical reconstruction of an inhomogeneity in an elliptic equation*, Inverse Probl. Sci. Eng. 22 (2014), 184–198.

[7] W. Fang and E. Cumberbatch, *Inverse problem for metal oxide semiconductor field-effect transistor contact resistivity*, SIAM J. Appl. Math. 53 (1992), 699–709.

[8] G. Feng, M. Li, and C. S. Chen, *On the ill-conditioning of the MFS for irregular boundary data with sufficient regularity*, Eng. Anal. Bound. Elem. 41 (2014), 98–102.

[9] C. Gáspár and A. Karageorghis, *Method of fundamental solutions formulations for biharmonic problems*, Eng. Anal. Bound. Elem. 175 (2025), Article ID 106180.

[10] A. Goravarty, D. J. Hawrysz, R. Roy, E. M. Sevick-Muraca, and M. J. Eppstein, *Influence of the refractive index-mismatch of the boundaries measured in fluorescence-enhanced frequency-domain photon migration imaging*, Opt. Express 10 (2002), 650–653.

[11] J. C. Hauge and D. Crowdy, *A new approach to the complex Helmholtz equation with applications to diffusion wave fields, impedance spectroscopy and unsteady Stokes flow*, IMA J. Appl. Math. 86 (2021), 1287–1326.

[12] F. Hettlich and W. Rundell, *Recovery of the support of a source term in an elliptic differential equation*, Inverse Probl. 13 (1997), 959–976.

[13] B. T. Johansson and D. Lesnic, *A method of fundamental solutions for transient heat conduction in layered materials*, Eng. Anal. Bound. Elem. 33 (2009), 1362–1367.

[14] A. Joshi, W. Bangerth, K. Hwong, J. Rasmussen, and E. M. Sevick-Muraca, *Fully adaptive FEM based fluorescence optical tomography from time-dependent measurements with area illumination and detection fluorescence tomography with adaptive finite elements*, Med. Phys. 33 (2006), 1299–1310.

[15] A. Joshi, W. Bangerth, K. Hwong, J. Rasmussen, and E. M. Sevick-Muraca, *Plane wave fluorescence tomography with adaptive finite elements*, Opt. Lett. 31 (2006), 193–195.

[16] A. Joshi, W. Bangerth, and E. M. Sevick-Muraca, *Adaptive finite element based tomography for fluorescence optical imaging of tissue*, Opt. Express 12 (2004), 5402–5417.

[17] A. JOSHI, W. BANGERTH, AND E. M. SEVICK-MURACA, *Non-contact fluorescence optical tomography with scanning patterned illumination*, Opt. Express 14 (2006), 6516–6534.
[18] H. KANG, K. KWON, AND K. YUN, *Recovery of an inhomogeneity in an elliptic equation*, Inverse Probl. 17 (2001), 25–44.
[19] A. KARAGEORGHIS AND C. S. CHEN, *Multi-level method of fundamental solutions for solving polyharmonic problems*, J. Comput. Appl. Math. 456 (2025), Article ID 116220.
[20] A. KARAGEORGHIS AND D. LESNIC, *The method of fundamental solutions for optical fluorescence*, Ann. Appl. Math. 41 (2025), 219–238.
[21] A. KARAGEORGHIS, D. LESNIC, AND L. MARIN, *The method of fundamental solutions for the identification of a scatterer with impedance boundary condition in interior inverse acoustic scattering*, Eng. Anal. Bound. Elem. 92 (2018), 218–224.
[22] A. KARAGEORGHIS, D. LESNIC, AND L. MARIN, *An efficient moving pseudo-boundary MFS for void detection*, Eng. Anal. Bound. Elem. 147 (2023), 90–111.
[23] S. KIM, *Uniqueness determination of inhomogeneity in an elliptic equation*, Inverse Probl. 18 (2002), 1325–1332.
[24] S. KIM AND M. YAMAMOTO, *Uniqueness in the identification of the support of a source term in an elliptic equation*, SIAM J. Math. Anal. 35 (2003), 148–159.
[25] L. MARIN, L. ELLIOTT, D. B. INGHAM, AND D. LESNIC, *The boundary element method for the numerical recovery of a circular inhomogeneity in an elliptic equation*, Eng. Anal. Bound. Elem. 28 (2004), 413–419.
[26] P. A. RAMACHANDRAN, *Method of fundamental solutions: Singular value decomposition analysis*, Commun. Numer. Meth. En. 18 (2002), 789–801.
[27] Y.-S. SMYRLIS AND A. KARAGEORGHIS, *Efficient implementation of the MFS: The three scenarios*, J. Comput. Appl. Math. 227 (2009), 83–92.